**Geomechanics and Engineering**, *Vol. 40, No. 2 (2025) 79-88*
https://doi.org/10.12989/gae.2025.40.2.079


# Influence of corrugation on SH wave propagation in rotating and initially stressed functionally graded magneto-electro-elastic substrate

K. Hemalatha[a], S. Kumar* and A. Akshaya[b]

*Department of Mathematics, College of Engineering and Technology, SRM Institute of Science and Technology, Kattankulathur-603203, India*

(*Received January 25, 2024, Revised December 20, 2024, Accepted January 2, 2025*)

**Abstract.** The shear horizontal (SH) waves in a rotating system comprising an initially stressed magneto-electro-elastic substrate were studied analytically. The upper boundary of substrate is taken as corrugated and stress free. With respect to electrically and magnetically upper boundary considered as two cases electrically and magnetically open and electrically and magnetically short. Dispersion equations have been obtained for electrically open and magnetically open and also electrically and magnetically short situations with corrugated interface. Based on the numerical results, the properties of SH waves through the proposed framework and the conditions depending on various physical and geometrical parameters have been examined. The study examines the simultaneous simulated results of several physical parameters, including rotation, inhomogeneity, phase velocity, initial stress, and corrugated SH wave interface distribution in the structure under consideration, which were created using Mathematica 7. The examined model could be helpful for the development of surface acoustic wave (SAW) devices.

**Keywords:** corrugation; inhomogeneity; initial stress; magneto-electro-elastic material; phase velocity; rotation; wave number

## 1. Introduction

Magneto-electro-elastic (MEE) materials are mixtures that display three distinct electromagnetic properties: magneto-electric, magneto-elastic (piezoelectric), and electro-elastic (piezomagnetic). By mixing piezoelectric and piezomagnetic particles inside an elastic matrix, where the strain field relates the piezoelectric phase's electric field to the piezomagnetic phase's magnetic field, such composites are created. These three-phase composites are better than two-phase ones in terms of magneto-electro-elastic properties. Van Suchtelen (1972) created the first artificial magneto-electro-elastic material artificially by mixing piezoelectric and piezomagnetic materials. According to Van Run *et al.* (1974), the $BaTiO_3$-$CoFe_2O_4$ composite they created had the most potent electromagnetic effect available at the time. Later, Bracke and Van Vliet (1981) discovered a broad magneto-electric transducer made of a composite material. Inhomogeneity issues with magneto-electro-elastic multi-inclusions and their applications in composite materials were encountered by Li (2000). The Green's function for anisotropic magnetoelastic solids having an oval cavity or a crack was covered by Jinxi *et al.* (2001). Authors such as Pan and Han (2005), Bhangake and Ganesan (2006), and Huang *et al.* (2007) discussed the functionally graded MEE materials using various solutions methods. Wave propagation on magneto-electro-elastic multilayered plates was observed by Chen *et al.* (2007). In MEE Materials, Arman (2007) investigated twelve shear surface waves steered by clamped or unconstrained limits. Surface electro-elastic SH waves in a layered device with a piezoelectric substrate and a harddielectric layer were described by Danoyan and Piliposian (2008). Li and Wei (2014a, b) encountered the pre-stressed and MEE solids' impact on the surface wave speed and velocity of functionally graded magneto-electro-elastic (FGMEE) materials. In their study, Wu *et al.* (2010) used the modified Pagano approach to analyze the three-dimensional static behavior of FGMEE plates. Anisotropic FGMEE beams exposed to arbitrary loading were the focus of a static analysis study by Huang *et al.* (2010). Zhao and Chen (2010) discussed using the symplectic framework for plane research for FGMEE materials. Chen *et al.* (2017) noticed wave propagation with a nonlocal influence in MEE multilayered plates. Yang *et al.* (2018) talked about applying analytical and finite element methods to analyze the natural properties of multilayered magneto-electro-elastic plates. Vinyas (2021) covered the computational analysis of intelligent magneto-electro-elastic materials and structures. To represent the propagation of elastodynamic waves in composites made of elastic, piezoelectric, and magneto-electro-elastic materials, Othmani *et al.* (2022) used orthogonal polynomial methods. In a magneto-electro-elastic layered structure with such a non-perfect and locally perturbed interface, Chaki and Bravo-Castillero (2023) investigated the statistical modeling of anti-plane surface waves. The propagation of Rayleigh waves in a FGPM layer over an elastic substrate was examined by Hemalatha *et al.* (2023). The SH-wave was examined by Hemalatha *et*

*Corresponding author, Assistant Professor
E-mail: santosh453@gmail.com
[a]Ph.D.
[b]Ph.D.



ISSN: 2005-307X (Print), 2092-6219 (Online)

*al.* (2024) in a heterogeneous semi-infinite material sandwiched by an initially stressed anisotropic ME layer. Ebrahimi *et al.* (2022) examined the impact of a magnetic field on the wave propagation behavior of a functionally graded beam resting on an elastic foundation within a thermal environment. Ebrahimi and Sepahvand (2024) conducted a wave propagation analysis of a cylindrical sandwich shell with an auxetic core, employing the first-order shear deformation theory. Eroglu *et al.* (2024a) analyzed the impact of a magnetic field on thermomechanical flexural wave propagation in embedded sandwich nanobeams. Eroglu *et al.* (2024b) analyzed the thermal vibration and buckling behavior of FGMEE porous higher-order nanobeams utilizing nonlocal strain gradient theory. Koc *et al.* (2024) analyzed the thermomechanical vibration behavior of nanoplates featuring FGMEE porous core, employing nonlocal strain gradient elasticity.

On the other hand, ageing of glue applied to two conjunct solids, microdefects, difusion impurities, and other types of damages frequently result in inadequate bonding at the interface of folded structures. Huang *et al.* (2009) came upon a two-phase piezoelectric/piezomagnetic system with an unsatisfactory interface that was propagating interfacial shear horizontal (SH) waves. Li and Lee (2010) explained about how a defected interface affects how a cylindrical piezoelectric sensor's SH wave propagates. Liu *et al.* (2010) studied the SH surface wave via a multilayer piezoelectric half-space with an imperfect contact. Sun *et al.* (2011) remarked about how the SH wave in a multiferroic composite is affected by the imperfect interface and piezoelectric/piezomagnetic stiffening. On a MEE heterostructure with defective interfaces, Otero *et al.* (2011) encountered the dispersion laws for SH waves. SH waves propagating in an imperfectly interfaced piezoelectric–piezomagnetic bilayer system were reported by Nie *et al.* (2012). The reflection and transmission coefficients of the SH mode in adhesive systems with defective interfaces were examined by Ding *et al.* (2016). The reflection and transmission of SH-waves across a corrugated interface between two semi-infinite anisotropic magnetoelastic half-spaces were examined by Kumar *et al.* (2017). In a piezoelectric/piezomagnetic plate with an unsatisfactory magnetoelectroelastic interface, Pang *et al.* (2019) investigated the propagation of SH waves. In material layers with imperfect interfaces, Singhal *et al.* (2019) investigated the influence of starting and couple stresses on the transmission of surface waves. In multilayered piezoelectric semiconductor plates with defective interfaces, Tian *et al.* (2020) investigated the SH waves. Interfacial defects impact on SH-wave propagation in a porous piezoelectric composite was examined by Rakshit *et al.* (2022). Circumferential SH waves in piezo-reinforced composite structures with imperfect interface bonding were the subject of discussion by Kumawat and Vishwakarma (2023). The Rayleigh wave at the imperfectly corrugated contact in the FGPM structure was examined by Hemalatha *et al.* (2023). Akshaya *et al.* (2024a) examined the behavior of transverse waves at an imperfectly corrugated interface within a functionally graded structure. Akshaya *et al.* (2024b) explored the propagation of SH waves in MEE structures with mechanically imperfect interfaces. Hemalatha and Kumar (2024) explored the propagation of SH waves in a rotating FGMEE with an imperfect interface structure.

Some researchers in past have investigated different problem of rotating media. In a rotating anisotropic elastic half-space, Ting (2004) investigated the surface waves. In magneto-thermoelastic medium, Sharma and Thakur (2006) examined the impact of rotation on Rayleigh-Lamb waves. The impact of rotation on Rayleigh waves in piezothermoelastic half space was examined by Sharma and Walia (2007). Sharma *et al.* (2008) talked about how Rayleigh waves in piezothermoelastic half space are affected by rotation and thermal relaxation. The secular equation of SH waves propagating in a pre-stressed, rotating piezo-composite structure with an imperfect contact was studied by Chaudhary *et al.* (2018). The investigation of interfacial imperfection in pre-stressed rotating multiferroic cylindrical tubes using an analytical method to wave vibration was presented by Chaudhary *et al.* (2019). Singh (2021) talked about the wave propagation in a nonlocal elastic, incompressible, rotating, transversely isotropic material.

This paper describes the propagation of SH wave in a rotating functionally graded magneto-electro-elastic (FGMEE) substrate system comprising with vacuum and FGMEE varying exponentially with corrugated interface, which is yet unaddressed for study as far as the known available literature. Previous studies primarily focused on investigating the secular equation of SH waves propagating in pre-stressed and rotating piezo-composite structures. The upper boundary of substrate is taken as corrugated and stress free. With respect to electrically and magnetically upper boundary considered as two cases electrically and magnetically open and electrically and magnetically short. Dispersion equations have been obtained for electrically open and magnetically open and also electrically and magnetically short situations with corrugated interface. Based on the numerical results, the properties of SH waves through the proposed framework and the conditions depending on various physical and geometrical parameters have been examined. The study examines the simultaneous simulated results of several physical parameters, including rotation, inhomogeneity, phase velocity, initial stress, and corrugated SH wave interface distribution in the structure under consideration.

## 2. Formulation of the problem

We have considered the corrugated, pre-stressed FGMEE substrate as shown in Fig. 1. The system Cartesian coordinates are taken so that the $x$-axis is vertically downward and the $y$-axis is in the direction of SH wave propagation along the interface between the FGMEE substrate and vacuum. And the system is rotating along the $y$-axis. It is thought that the layer is upper surface lacks traction. At $x=g(y)$ is the boundary surface of the substrate, where $g(y)$ is a continuous periodic function of $y$ that is independent of $x$.

The definition of the Fourier series of $g(y)$ using an appropriate origin of coordinates is

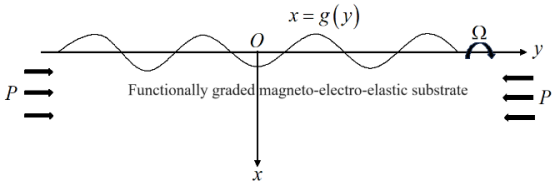


Fig. 1 Geometry of the problem

$$g=\sum_{n=1}^{\infty}\left[g_n e^{in\lambda y}+g_{-n}e^{-in\lambda y}\right] \tag{1}$$

where $n$ is the order of the series expansion and $g_n$ and $g_{-n}$ are the Fourier expansions coefficients. The constants $a,b,R_n,I_n$ will be introduced as follows

$$g_{\pm 1}=\frac{a}{2},\ g_{\pm n}=\frac{R_n \mp I_n}{2},\ \ n=2,3,... \tag{2}$$

and

$$\begin{aligned} g=&a\cos\lambda y+R_2\cos 2\lambda y+I_2\sin n\lambda y+...\\ &+R_n\cos n\lambda y+I_n\sin n\lambda y+... \end{aligned} \tag{3}$$

in which cosine but also sine Fourier coefficients are represented by $R_n$ and $I_n$ correspondingly. The boundary surfaces of the substrate expressed in terms of cosine i.e. $g=a\cos\lambda y$.

The Gauss law of magneto-electrostatics without free charge and the equilibrium equations of elasticity for linearly magneto-electro-elastic materials without body forces are as follows:

$$\begin{aligned} &T_{ij,j}+\left(u_{i,k}\,P_{kj}\right)_{,j}\\ &\quad=\rho_i\left(\ddot{u}+\left(\Omega\times\Omega\times u\right)+\left(2\Omega\times\dot{u}\right)\right)_j\\ &D_{i,i}+\left(u_{i,j}\,D_j^0\right)_{,i}=0\\ &B_{i,i}+\left(u_{i,j}\,B_j^0\right)_{,i}=0 \end{aligned} \tag{4}$$

where *i,j=1,2,3*. The comma "," indicates space-coordinate differentiation and the dots "." indicate space-time differentiation in Eq. (4).

For a linearly magneto-electro-elastic solid that is anisotropic, the linked constitutive relation can be expressed as

$$\begin{aligned} T_{ij}&=C_{ijkl}S_{kl}-e_{kij}E_k-h_{kij}H_k\\ D_i&=e_{ikl}S_{kl}+\kappa_{il}E_i+\beta_{il}H_l\\ B_i&=h_{ikl}S_{kl}+\beta_{il}E_l+\mu_{il}H_l \end{aligned} \tag{5}$$

The following is the relation between mechanical displacement and strain components

$$S_{ij}=\frac{1}{2}\left(u_{i,j}+u_{j,i}\right) \tag{6}$$

Quasi-static approximation of the Maxwell equations yields

$$E_i=-\phi_{,i},\ H_i=-\psi_{,i} \tag{7}$$

Let *(u, v, w)* represent a particle's displacement components in the *(x,y,z)* directions, respectively. The *z*-axis does not affect the displacement or potential electrical components since the SH wave only causes displacement in the *z*-direction and propagates in the *y*-direction and with the initial stress component *P*. As a result, we can take the mechanical displacement components, the electric and magnetic potential as

$$\begin{aligned} &u=0,v=0,w=w(x,y,t),\\ &\phi=\phi(x,y,t),\psi=\psi(x,y,t) \end{aligned} \tag{8}$$

The governing equations for rotating with initially stressed FGMEE substrate are obtained by applying Eqs. (4)-(8),

$$\begin{aligned} &C_{44}^{(m)}\nabla^2 w_m+P\frac{\partial^2 w_m}{\partial y^2}+e_{15}^{(m)}\nabla^2\phi_m+h_{15}^{(m)}\nabla^2\psi_m\\ &\quad+C_{44}^{\prime(m)}\frac{\partial w_m}{\partial x}+e_{15}^{\prime(m)}\frac{\partial\phi_m}{\partial x}+h_{15}^{\prime(m)}\frac{\partial\psi_m}{\partial x}\\ &\quad=\rho_m\left[\frac{\partial^2 w_m}{\partial t^2}-\Omega^2 w_m+2\Omega\frac{\partial w_m}{\partial t}\right],\\ &e_{15}^{(m)}\nabla^2 w_m-\kappa_{11}^{(m)}\nabla^2\phi_m-\beta_{11}^{(m)}\nabla^2\psi_m\\ &\quad+e_{15}^{\prime(m)}\frac{\partial w_m}{\partial x}-\kappa_{11}^{\prime(m)}\frac{\partial\phi_m}{\partial x}-\beta_{11}^{\prime(m)}\frac{\partial\psi_m}{\partial x}=0,\\ &h_{15}^{(m)}\nabla^2 w_m-\beta_{11}^{(m)}\nabla^2\phi_m-\mu_{11}^{(m)}\nabla^2\psi_m\\ &\quad+h_{15}^{\prime(m)}\frac{\partial w_m}{\partial x}-\beta_{11}^{\prime(m)}\frac{\partial\phi_m}{\partial x}-\mu_{11}^{\prime(m)}\frac{\partial\psi_m}{\partial x}=0 \end{aligned} \tag{9}$$

where $\nabla$ is the two dimensional Laplacian operator.

The rotating pre-stressed FGMEE substrate material characteristics are expected to be positively exponentially distributed across the depth (*x*-axis). The rotating pre-stressed FGMEE substrate functional gradients are therefore regarded as

$$\begin{aligned} &C_{44}^{(m)}(x)=C_{44}^{(m0)}e^{\alpha x},e_{15}^{(m)}(x)=e_{15}^{(m0)}e^{\alpha x},\\ &h_{15}^{(m)}(x)=h_{15}^{(m0)}e^{\alpha x},\kappa_{11}^{(m)}(x)=\kappa_{11}^{(m0)}e^{\alpha x},\\ &\beta_{11}^{(m)}(x)=\beta_{11}^{(m0)}e^{\alpha x},\ \mu_{11}^{(m)}(x)=\mu_{11}^{(m0)}e^{\alpha x},\\ &\rho=\rho^{(m0)}e^{\alpha x},P=P^{(m0)}e^{\alpha x}. \end{aligned} \tag{10}$$

By employing (10) in Eq. (9) we get

$$\begin{aligned} &C_{44}^{(m0)}\left(\nabla^2 w_m+\alpha\frac{\partial w_m}{\partial x}\right)+P^{(m0)}\frac{\partial^2 w_m}{\partial y^2}\\ &+e_{15}^{(m0)}\left(\nabla^2\phi_m+\alpha\frac{\partial\phi_m}{\partial x}\right)\\ &+h_{15}^{(m0)}\left(\nabla^2\psi_m+\alpha\frac{\partial\psi_m}{\partial x}\right)\\ &=\rho^{(m0)}\left[\frac{\partial^2 w_m}{\partial t^2}-\Omega^2 w_m+2\Omega\frac{\partial w_m}{\partial t}\right],\\ &e_{15}^{(m0)}\left(\nabla^2 w_m+\alpha\frac{\partial w_m}{\partial x}\right)-\kappa_{11}^{(m0)}\left(\nabla^2\phi_m+\alpha\frac{\partial\phi_m}{\partial x}\right)\\ &-\beta_{11}^{(m0)}\left(\nabla^2\psi_m+\alpha\frac{\partial\psi_m}{\partial x}\right)=0,\\ &h_{15}^{(m0)}\left(\nabla^2 w_m+\alpha\frac{\partial w_m}{\partial x}\right)-\beta_{11}^{(m0)}\left(\nabla^2\phi_m+\alpha\frac{\partial\phi_m}{\partial x}\right)\\ &-\mu_{11}^{(m0)}\left(\nabla^2\psi_m+\alpha\frac{\partial\psi_m}{\partial x}\right)=0 \end{aligned} \tag{11}$$

where the FGMEE substrate is specified by the superscripts(subscripts) *m*.

Furthermore, the Laplace equation is satisfied by the magnetic and electric potentials in the air above the layer $(x < g(y))$.

$$\nabla^2\phi_v = 0,\ \nabla^2\psi_v = 0 \tag{12}$$

where potential is represented by the subscript *v* in the vacuum.

## 3. Solution treatment

### 3.1 Solution treatment for FGMEE substrate

In order to solve the Eq. (11) introducing the following two functions

$$\phi' = \phi_m - \zeta w_m,\ \psi' = \psi_m - \eta w_m \tag{13}$$

Substitution of Eq. (13) into Eq. (11) yields,

$$\begin{aligned}
&\overline{C_{44}^{(m0)}}\left(\nabla^2 w_m + \alpha\frac{\partial w_m}{\partial x}\right) + P^{(m0)}\frac{\partial^2 w_m}{\partial y^2} \\
&= \rho^{(m0)}\left[\frac{\partial^2 w_m}{\partial t^2} - \Omega^2 w_m + 2\Omega\frac{\partial w_m}{\partial t}\right] \\
&\nabla^2\phi' + \alpha\frac{\partial\phi'}{\partial x} = 0 \\
&\nabla^2\psi' + \alpha\frac{\partial\psi'}{\partial x} = 0
\end{aligned} \tag{14}$$

where

$$\zeta = \frac{\mu_{11}^{(m0)}e_{15}^{(m0)} - \beta_{11}^{(m0)}h_{15}^{(m0)}}{\kappa_{11}^{(m0)}\mu_{11}^{(m0)} - \left(\beta_{11}^{(m0)}\right)^2},$$

$$\eta = \frac{\kappa_{11}^{(m0)}h_{15}^{(m0)} - \beta_{11}^{(m0)}e_{15}^{(m0)}}{\kappa_{11}^{(m0)}\mu_{11}^{(m0)} - \left(\beta_{11}^{(m0)}\right)^2},$$

and

$$\begin{aligned}
\overline{C_{44}^{(m0)}} = C_{44}^{(m0)} &+ \frac{\mu_{11}^{(m0)}\left(e_{15}^{(m0)}\right)^2 + \kappa_{11}^{(m0)}\left(h_{15}^{(m0)}\right)^2}{\kappa_{11}^{(m0)}\mu_{11}^{(m0)} - \left(\beta_{11}^{(m0)}\right)^2} \\
&- \frac{2\beta_{11}^{(m0)}e_{15}^{(m0)}h_{15}^{(m0)}}{\kappa_{11}^{(m0)}\mu_{11}^{(m0)} - \left(\beta_{11}^{(m0)}\right)^2}
\end{aligned}$$

Due to time-harmonic dependency of SH wave propagation, the solution of Eq. (14) can be assumed as

$$\begin{aligned}
&\{w_m, \phi', \psi'\}(x, y, t) \\
&= \{W_m, \Phi_m, \Psi_m\}(x)e^{ik(y-ct)}
\end{aligned} \tag{15}$$

In light of Eq. (15), Eq. (14) reduce to the following

$$\begin{aligned}
&\overline{C_{44}^{(m0)}}\nabla^2 W_m - k^2 P^{(m0)}W_m + \alpha\frac{\partial W_m}{\partial x} \\
&= \rho^{(m0)}\left[-k^2c^2W_m - \Omega^2 W_m + 2ikc\Omega W_m\right], \\
&\nabla^2\Phi_m + \alpha\frac{\partial\Phi_m}{\partial x} = 0, \\
&\nabla^2\Psi_m + \alpha\frac{\partial\Psi_m}{\partial x} = 0.
\end{aligned} \tag{16}$$

Now, from Eq. (16), we can obtain the required mechanical displacement, potential function, and magnetic function for the rotating FGMEE substrate which is pre-stressed as

$$\begin{aligned}
w_m &= \left[Ae^{sx}\right]e^{ik(y-ct)} \\
\phi_m &= \left[B e^{tx} + \zeta Ae^{sx}\right]e^{ik(y-ct)} \\
\psi_m &= \left[C e^{tx} + \eta Ae^{sx}\right]e^{ik(y-ct)}
\end{aligned} \tag{17}$$

where *A, B, C* are unknown constants and *s, t* are defined in *Appendix*.

### 3.2 Solution treatment for vacuum

The solution to Eq. (12) is obtained by, assuming that the electric potential function $\phi_v$ and magnetic potential function $\psi_v$ diminishes as $x \to -\infty$,

$$\begin{aligned}
\phi_v &= D e^{kx}e^{ik(y-ct)} \\
\psi_v &= E e^{kx}e^{ik(y-ct)}
\end{aligned} \tag{18}$$

where *D*, *E* are unknown constants.

## 4. Boundary conditions

The layer is perfectly bonded with elastic substrate whereas upper boundary as stress free. At the interface, scalar potential, electrical displacement and mechanical displacement are continuous functions. These conditions are illustrated mathematically below,

1. The mechanical stress-free condition at $x = g(y)$ is

$$T_{31}^{(m)} - g'T_{23}^{(m)} = 0 \tag{19}$$

where $g' = \frac{dg}{dy}$.

2. Electrical boundary condition at $x = g(y)$ are
   i) Electrically open case:

$$D_1^{(m)} = D_1^{(v)},\ \phi_m = \phi_v \tag{20}$$

   ii) Electrically short case:

$$\phi_m = 0 \tag{21}$$

3. Magnetic boundary condition at $x = g(y)$ are
   i) Magnetically open case:

$$B_1^{(m)} = B_1^{(v)},\ \psi_m = \psi_v \tag{22}$$

   ii) Magnetically short case:

$$\psi_m = 0 \tag{23}$$

## 5. Dispersion relations

### 5.1 Electrically Open and Magnetically Open (EOMO)

Table 1 Material coefficients of the Magneto-electro-elastic substrate $BaTiO_3$-$CoFe_2O_4$

| Materials | Elastic constant $C_{44}(10^{10}N/m^2)$ | Piezoelectric constant $e_{15}(C/m^2)$ | Piezomagnetic constant $h_{15}(N/Am)$ | Magnetic constant $\mu_{11}(10^{-6}Ns^2C^{-2})$ | Dielectric constant $\kappa_{11}(10^{-9}C/Vm)$ | Magnetoelectric constant $\beta_{11}(10^{-9}Ns/VC)$ | Mass density $\rho(10^3\ kg/m^3)$ |
|---|---|---|---|---|---|---|---|
| $BaTiO_3$-$CoFe_2O_4$ | 4.8 | 0.08 | 238 | -258 | 0.19 | 0.005 | 7.50 |

With the initially stressed FGMEE substrate, vacuum, and their corresponding mechanical, electric, and magnetic components yielded into boundary conditions (19), (20), and (22) using these boundary conditions with solutions (17), and (18), we obtain the homogeneous equation of unknown constants A, B, C, D and E.

The dispersion relation for a rotating FGMEE substrate which is initially stressed with a free-from-top boundary condition can be found in fifth-order determinant format by taking out the constants A, B, C, D and E.

$$\left|\gamma_{ij}\right| = 0 \tag{24}$$

where $i, j=1,2,...,5$ and the definition of $\gamma_{ij}$ is presented in the *Appendix*.

### *5.2 Electrically Short and Magnetically Short (ESMS)*

With the initially stressed FGMEE substrate, and their corresponding mechanical, electric, and magnetic components yielded into boundary conditions (19), (21), and (23) using these boundary conditions with solutions (17), and (18), we obtain the homogeneous equation of unknown constants A, B, and C.

The dispersion relation for a rotating FGMEE substrate which is initially stressed with a free-from-top boundary condition can be found in third-order determinant format by taking out the constants A, B, and C.

$$\left|\delta_{ij}\right| = 0 \tag{25}$$

where $i,j=1,2,3$ and the definition of $\delta_{ij}$ is presented in the *Appendix*.

## 6. Numerical example and discussion

The analytical solution of the assumed structure reached dispersion relations. From, dispersion relations, wave propagation characteristics have been thoroughly studied by the influence on phase velocity on the various parameters in the FGMEE substrate. For the two scenarios: EOMO and ESMS the relationships between phase velocity and wave number are found.

For this study, we consider the magneto-electro-elastic material $BaTiO_3$-$CoFe_2O_4$. In Table 1, the summarises all of the material constants used in this article. $\kappa_v = 8.85\times10{-}12$ F/m and $\mu_v = 4\pi \times10{-}7\ Ns^2C^{-2}$ are the dielectric constant and magnetic permittivity of vacuum, respectively.

Figs. 2-9 illustrate how the plane SH wave propagates in the rotating structure of the FGMEE substrate according to the rotating parameter, initial stress, inhomogeneity parameter, and corrugation amplitude. All graphs present the dispersion curves for both open and short situations for phase velocity change and wave number. Generally speaking, all graphs take into account the parameter default values as $\alpha = 50, \Omega = 1000$, $a = 0.005$, $P$=100 GPa unless otherwise specified. $P$ is used for the initial stress for substrate instead of $P^{(m0)}$ in the discussion arising preceding it and in the graphics.

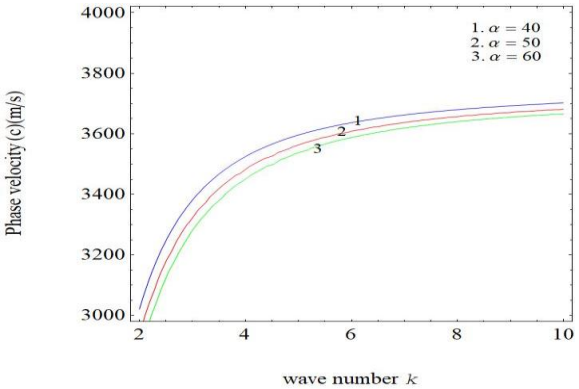


Fig. 2 Variations in wave number & phase velocity for EOMO situation with changing values of α

### *6.1 For the effect of EOMO situation*

The graphical representation of the effects of the rotation parameter, corrugation amplitude, inhomogeneity parameter, and initial stress on phase velocity is presented for the EOMO scenario. Figs. 2-5 illustrate that variations in wave number with phase velocity significantly influence the propagation of SH waves within the examined structure. Fig. 2 shows the relationship between phase velocity and wave number for different values of the inhomogeneity parameter, *α (40, 50, 60)*. It is observed that as α decreases, the phase velocity $c$ increases with wave number $k$. The influence of α is particularly evident. Fig. 3 demonstrates the effect of phase velocity and wave number for various values of the rotation parameter, Ω (500, 1000, 1500). As the wave number $k$ increases, phase velocity gradually rises for different Ω values. For all values of $k$, phase velocity increases as Ω decreases, and the curves exhibit a consistent upward trend for all values of Ω. Fig. 4 shows the relationship between phase velocity and wave number for corrugation amplitudes of ($a$ = *0.002, 0.005*, and *0.008*. As seen in Fig. 4, the phase velocity of SH waves increases with higher corrugation amplitudes. Fig. 5 demonstrates how phase velocity changes with respect to wave number for different initial stress values in the substrate, $P$ = *100* GPa, *200* GPa, and *300* GPa. As the wave number $k$ increases, the phase velocity also increases for all values of $P$, and for each $k$, the phase velocity continues to rise as the value of $P$ grows.

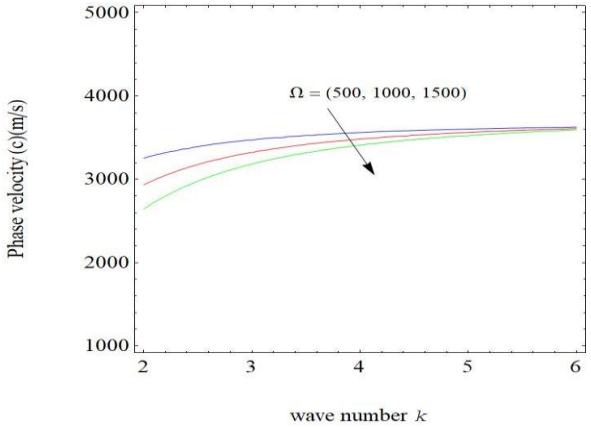


Fig. 3 Variations in wave number & phase velocity for EOMO situation with changing values of Ω

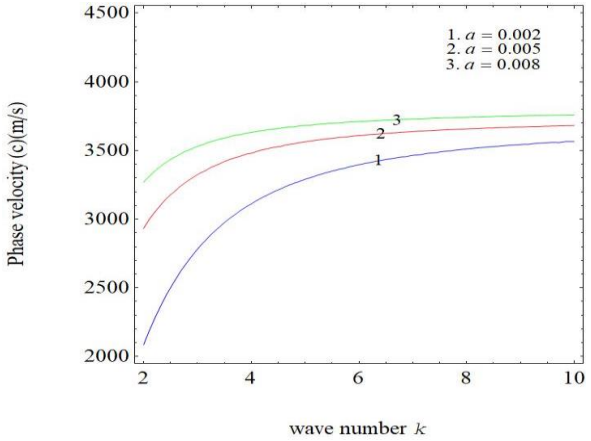


Fig. 4 Variations in wave number & phase velocity for EOMO situation with changing values of *a*

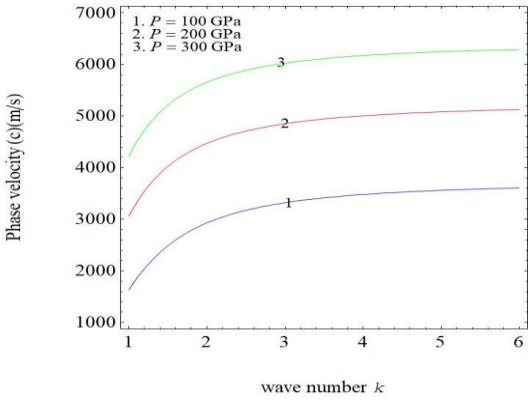


Fig. 5 Variations in wave number & phase velocity for EOMO situation with changing values of *P*

### *6.2 For the effect of ESMS situation*

The same material system used in the EOMO case is also considered for the electrically and magnetically short cases. The variations in wave number and phase velocity, illustrated in Figs. 6 to 9, significantly influence the propagation of the SH wave within this structure. Fig. 6 depicts the relationship between phase velocity and wave number for different values of the inhomogeneity parameter, α (40, 50, 60). The shape of these curves is similar to those in Fig. 2, but the effect is more pronounced in this case. Fig. 7, on the other hand, shows the relationship between phase velocity and wave number for various values of the rotating parameter, Ω (500, 1000, 1500).

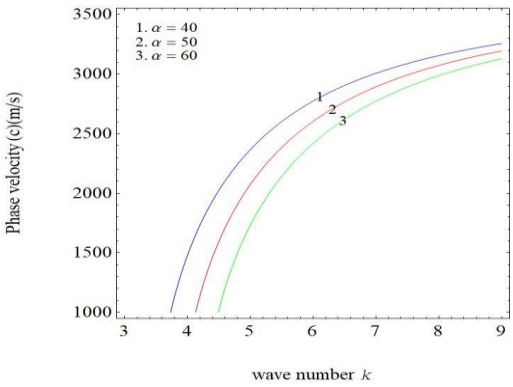


Fig. 6 Variations in wave number & phase velocity for ESMS situation with changing values of α

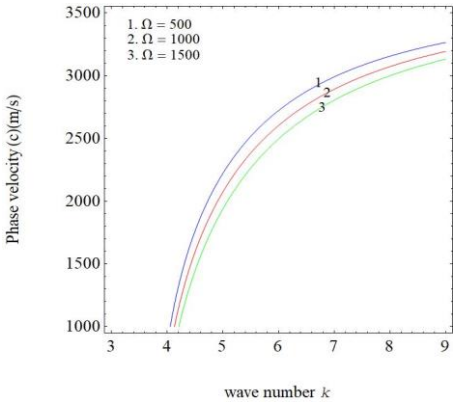


Fig. 7 Variations in wave number & phase velocity for ESMS situation with changing values of Ω

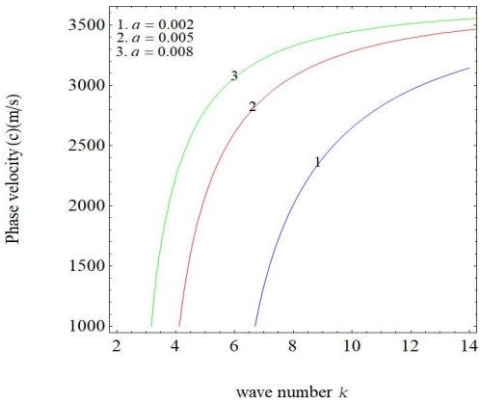


Fig. 8 Variations in wave number & phase velocity for ESMS situation with changing values of *a*

The curves in this case exhibit a steady increase. Fig. 8 illustrates the relationship between phase velocity and wave number for different corrugation amplitudes, specifically *(a = 0.002, 0.005, 0.008)*. This behavior is similar to that observed in Fig. 4, though the effect is more pronounced in this case. Additionally, Fig. 9 demonstrates the influence of phase velocity as it relates to wave number for varying initial substrate stress values, (*P = 100* GPa, *200* GPa, *300* GPa). The

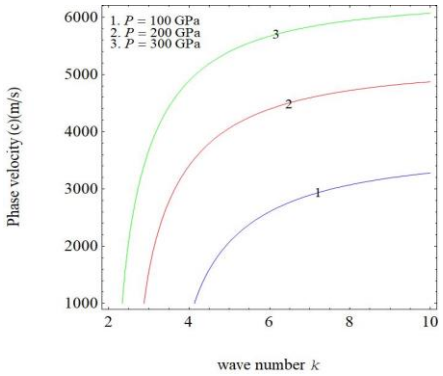


Fig. 9 Variations in wave number & phase velocity for ESMS situation with changing values of *P*

impact of initial stress on phase velocity is notably more significant, highlighting its stronger effect in comparison to the other factors.

## 7. Conclusions

This study theoretically investigates the propagation of SH waves in a rotating structure with an initially stressed FGMEE substrate that features a corrugated interface. The dispersion relations for the EOMO and ESMS cases have been derived in determinant form, considering the influence of the corrugated interface. Numerical calculations of the phase velocity of the SH wave are performed. For a specific model, it was observed that the phase velocity of the SH wave varies noticeably based on the parameters of the model under consideration. Based on these findings, the following conclusions can be drawn:

1. In the cases of both EOMO and ESMS configurations with a corrugated interface, various parameters significantly influence the phase velocity characteristics of the SH wave. These parameters alter the shape and behavior of the phase velocity curves, highlighting their sensitivity to changes in the physical and structural conditions of the medium.
2. Typically, the phase velocity of a SH wave tends to increase as the wave number becomes larger, indicating a direct relationship between the wave's propagation speed and its spatial frequency.
3. The findings indicate that, in each case, the phase velocity of the SH wave increases as the inhomogeneity parameter of the rotating FGMEE substrate decreases.
4. As the material's rotation parameter decreases in both scenarios, the phase velocity of the SH wave consistently increases, showing a continuous upward trend.
5. The amplitude of the upper boundary corrugation parameter affects the phase velocity of the SH wave, influencing the wave's propagation characteristics and altering the speed at which the wave travels through the medium.
6. As the initial stresses in the material rise, there is a gradual and consistent increase in the phase velocity of the SH wave.

This research has the potential to significantly benefit various devices, including rotation sensors, magneto-electro-elastic devices with functionally graded materials, and other similar technologies. Additionally, the findings contribute to the development of a new class of Surface Acoustic Wave (SAW) sensors, which exhibit improved performance, enhanced response, and increased sensitivity. These advancements could lead to more efficient and precise applications in various fields.

## Acknowledgments

One of the authors expresses gratitude to SRM Institute of Science and Technology, Kattankulathur, India, for providing the best research facilities and study time for us to conduct our research.

## References

Akshaya, A., Kumar, S. and Hemalatha, K. (2024a), "Behaviour of transverse wave at an imperfectly corrugated interface of a functionally graded structure", *Phys. Wave Phenomena*, **32**(2), 117-134. https://doi.org/10.3103/S1541308X24700067.

Akshaya, A., Kumar, S. and Hemalatha, K. (2024b), "Propagation of shear horizontal wave at magneto-electro-elastic structure subjected to mechanically imperfect interface", *Mech. Adv. Compos. Struct.*, **12**(1), 97-114. https://doi.org/10.22075/macs.2024.32653.1596.

Bhangale, R.K. and Ganesan, N. (2006), "Free vibration of simply supported functionally graded and layered magneto-electro-elastic plates by finite element method", *J. Sound Vib*, **294**(4-5), 1016-1038. https://doi.org/10.1016/j.jsv.2005.12.030.

Bracke, L.P. and Van Vliet, R.G. (1981), "A broadband magneto-electric transducer using a composite material", *Int. J. Electron. Theor. Exp.*, **51**(3), 255-262. https://doi.org/10.1080/00207218108901330.

Chaki, M.S. and Bravo-Castillero, J. (2023), "A mathematical analysis of anti-plane surface wave in a magneto-electro-elastic layered structure with non-perfect and locally perturbed interface", *Eur. J. Mech. A - Solid*, **97**, 104820. https://doi.org/10.1016/j.euromechsol.2022.104820.

Chaudhary, S., Sahu, S.A. and Singhal, A. (2018), "On secular equation of SH waves propagating in pre-stressed and rotating piezo-composite structure with imperfect interface", *J. Intel. Mat. Syst. Str.*, **29**(10), 2223-2235. https://doi.org/10.1177/1045389X18758192.

Chaudhary, S., Sahu, S.A., Singhal, A. and Nirwal, S. (2019), "Interfacial imperfection study in pres-stressed rotating multiferroic cylindrical tube with wave vibration analytical approach", *Mater. Res. Express*, **6**(10), 105704. https://doi.org/10.1088/2053-1591/ab3880.

Chen, J., Pan, E. and Chen, H. (2007), "Wave propagation in magneto-electro-elastic multilayered plates", *Int. J. Solids Struct.*, **44**(3-4), 1073-1085. https://doi.org/10.1016/j.ijsolstr.2006.06.003.

Chen, J., Guo, J. and Pan, E. (2017), "Wave propagation in magneto-electro-elastic multilayered plates with nonlocal effect", *J. Sound Vib.*, **400**, 550-563. https://doi.org/10.1016/j.jsv.2017.04.001.

Danoyan, Z.N. and Piliposian, G.T. (2008), "Surface electro-elastic shear horizontal waves in a layered structure with a piezoelectric substrate and a hard dielectric layer", *Int. J. Solids Struct.*, **5**(2), 431-441.

https://doi.org/10.1016/j.ijsolstr.2007.08.036.
Ding, J., Wu, B. and He, C. (2016), "Reflection and transmission coefficients of the SH0 mode in the adhesive structures with imperfect interface", *Ultrasonics*, **70**, 248-257. https://doi.org/10.1016/j.ultras.2016.05.010.
Ebrahimi, F., Seyfi, A., Nouraei, M. and Haghi P. (2022), "Influence of magnetic field on the wave propagation response of functionally graded (FG) beam lying on elastic foundation in thermal environment", *Waves Random Complex*, **32**(5), 2158-2176. https://doi.org/10.1080/17455030.2020.1847359.
Ebrahimi, F. and Sepahvand, M. (2024), "Wave propagation analysis of cylindrical sandwich shell with auxetic core utilizing first-order shear deformable theory (FSDT)", *Mech. Based Des. Struc.*, **52**(3), 1705-1729. https://doi.org/10.1080/15397734.2022.2159835.
Eroğlu, M., Esen, İ. and Koç, M.A. (2024a), "Effect of the magnetic field on the thermomechanical flexural wave propagation of embedded sandwich nanobeams", *Mech. Based Des. Struc.*, **22**, 1-33. https://dx.doi.org/10.1080/15397734.2024.2308659.
Eroğlu, M., Esen, İ. and Koç, M.A. (2024b), "Thermal vibration and buckling analysis of magneto-electro-elastic functionally graded porous higher-order nanobeams using nonlocal strain gradient theory", *Acta Mechanica*, **235**(2), 1175-211. https://dx.doi.org/10.1007/s00707-023-03793-y.
Hemalatha, K., Kumar, S. and Prakash, D. (2023), "Dispersion of Rayleigh wave in a functionally graded piezoelectric layer over elastic substrate", *Forces in Mech.*, **10**, 100171. https://doi.org/10.1016/j.finmec.2023.100171.
Hemalatha, K., Kumar, S. and Kim, I. (2024), "Study of SH-wave in a pre-stressed anisotropic magnetoelastic layer sandwich by heterogeneous semi-infinite media", *Math. Comput. Simul.*, **222**, 225-241. https://doi.org/10.1016/j.matcom.2023.08.021.
Hemalatha, K., Kumar, S. and Akshaya, A. (2023), "Rayleigh wave at imperfectly corrugated interface in FGPM structure", *Coupled Syst. Mech.*, **12**(4), 337. https://doi.org/10.12989/csm.2023.12.4.337.
Hemalatha, K. and Kumar, S. (2024), "Propagation of SH Wave in a Rotating Functionally Graded Magneto-Electro-Elastic Structure with Imperfect Interface", *J. Vib. Eng. Technol.*, **19**, 1-5. https://doi.org/10.1007/s42417-024-01365-5.
Huang, D.J., Ding, H.J. and Chen, W.Q. (2007), "Analytical solution for functionally graded magneto-electro-elastic plane beams", *Int. J. Eng. Sci.*, **45**(2-8), 467-485. https://doi.org/10.1016/j.ijengsci.2007.03.005.
Huang, D.J., Ding, H.J. and Chen, W.Q. (2010), "Static analysis of anisotropic functionally graded magneto-electro-elastic beams subjected to arbitrary loading", *Eur. J. Mech. A - Solid*, **29**(3), 356-369. https://doi.org/10.1016/j.euromechsol.2009.12.002.
Huang, Y., Li, X.F. and Lee, K.Y. (2009), "Interfacial shear horizontal (SH) waves propagating in a two-phase piezoelectric/piezomagnetic structure with an imperfect interface", *Philos. Mag. Lett.*, **89**(2), 95-103. https://doi.org/10.1080/09500830802555702.
Jinxi, L., Xianglin, L. and Yongbin, Z. (2001), "Green's functions for anisotropic magnetoelectroelastic solids with an elliptical cavity or a crack", *Int. J. Eng. Sci.*, **39**(12), 1405-1418. https://doi.org/10.1016/S0020-7225(01)00005-2.
Koç, M.A., Esen, İ. and Eroğlu, M. (2024), "Thermomechanical vibration response of nanoplates with magneto-electro-elastic face layers and functionally graded porous core using nonlocal strain gradient elasticity", *Mech. Adv. Mater. Struct.*, **31**(18), 4477-509. https://doi.org/10.1080/15376494.2023.2199412.
Kumar, S., Pal, P.C. and Majhi, S. (2017), "Reflection and transmission of SH-waves at a corrugated interface between two semi-infinite anisotropic magnetoelastic half-spaces", *Wave Random Complex*, **27**(2), 339-358. https://doi.org/10.1080/17455030.2016.1245454.
Kumawat, S. and Vishwakarma, S.K. (2023), "Circumferential SH wave in piezo-reinforced composite structure with imperfect interface bonding", *Appl. Math. Modell.*, **123**, 311-331. https://doi.org/10.1016/j.apm.2023.06.034.
Li, J.Y. (2000), "Magnetoelectroelastic multi-inclusion and inhomogeneity problems and their applications in composite materials", *Int. J. Eng. Sci.*, **38**(18), 1993-2011. https://doi.org/10.1016/S0020-7225(00)00014.
Li, Y.D. and Lee, K.Y. (2010), "Effect of an imperfect interface on the SH wave propagating in a cylindrical piezoelectric sensor", *Ultrasonics*, **50**(4-5), 473-478. https://doi.org/10.1016/j.ultras.2009.10.006.
Li, L. and Wei, P.J. (2014). "Surface wave speed of functionally graded magneto-electro-elastic materials with initial stresses", *J. Theor. Appl. Mech.*, **44**(3), 49-64. https://doi.org/10.2478/jtam-2014-0016.
Li, L. and Wei, P.J. (2014), "The piezoelectric and piezomagnetic effect on the surface wave velocity of magneto-electro-elastic solids", *J. Sound Vib.*, **333**(8), 2312-2326. https://doi.org/10.1016/j.jsv.2013.12.005.
Liu, J., Wang, Y. and Wang, B. (2010), "Propagation of shear horizontal surface waves in a layered piezoelectric half-space with an imperfect interface", *IEEE T. Ultrason. Ferr.*, **57**(8), 1875-1879. https://doi.org/10.1109/TUFFC.2010.1627.
Melkumyan, A. (2007), "Twelve shear surface waves guided by clamped/free boundaries in magneto-electro-elastic materials", *Int. J. Solids Struct.*, **44**(10), 3594-3599. https://doi.org/10.1016/j.ijsolstr.2006.09.016.
Nie, G., Liu, J., Fang, X. and An, Z. (2012), "Shear horizontal (SH) waves propagating in piezoelectric–piezomagnetic bilayer system with an imperfect interface", *Acta Mechanica*, **223**(9), 1999-2009. https://doi.org/10.1007/s00707-012-0680-6.
Otero, JA., Calas, H., Rodríguez-Ramos, R., Bravo, J., Aguiar, A. R. and Monsivais, G. (2011), "Dispersion relations for SH waves on a magnetoelectroelastic heterostructure with imperfect interfaces", *J. Mech. Mater. Struct.*, **6**(7), 969-993. https://doi.org/10.2140/jomms.2011.6.969.
Othmani, C., Zhang, H., Lu, C., Wang. Y.Q. and Kamali, A.R. (2022), "Orthogonal polynomial methods for modeling elastodynamic wave propagation in elastic, piezoelectric and magneto-electro-elastic composites—A review", *Compos. Struct.*, **286**, 115245. https://doi.org/10.1016/j.compstruct.2022.115245.
Pan, E. and Han, F. (2004), "Exact solution for functionally graded and layered magneto-electro-elastic plates", *Int. J. Eng. Sci.*, **43**(3-4), 321-339. https://doi.org/10.1016/j.ijengsci.2004.09.006.
Pang, Y., Feng, W., Liu, J. and Zhang, C. (2019), "SH wave propagation in a piezoelectric/piezomagnetic plate with an imperfect magnetoelectroelastic interface", *Wave Random Complex*, **29**(3), 580-94. https://doi.org/10.1080/17455030.2018.1539277.
Rakshit, S., Mistri, K.C., Das, A. and Lakshman, A. (2022), "Effect of interfacial imperfections on SH-wave propagation in a porous piezoelectric composite", *Mech. Adv. Mater. Struct.*, **29**(25), 4008-4018. https://doi.org/10.1080/15376494.2021.1916138.
Sharma, J.N. and Thakur, M.D. (2006), "Effect of rotation on Rayleigh–Lamb waves in magneto-thermoelastic media", *J. Sound Vib.*, **296**(4-5), 871-887. https://doi.org/10.1016/j.jsv.2006.03.014.
Sharma, J.N. and Walia, V. (2007), "Effect of rotation on Rayleigh waves in piezothermoelastic half space", *Int. J. Solids Struct.*, **44**(3-4), 1060-1072. https://doi.org/10.1016/j.ijsolstr.2006.06.005.
Sharma, J. N., Walia, V. and Gupta, S.K. (2008), "Effect of

rotation and thermal relaxation on Rayleigh waves in piezothermoelastic half space", *Int. J. Mech. Sci.*, **50**(3), 433-444. https://doi.org/10.1016/j.ijmecsci.2007.10.001.

Singh, B. (2021), "Propagation of waves in an incompressible rotating transversely isotropic nonlocal elastic solid", *Vietnam J. Mech.*, **43**(3), 237-252. https://doi.org/10.15625/0866-7136/15533.

Singhal, A., Sahu, S.A., Chaudhary, S. and Baroi, J. (2019), "Initial and couple stress influence on the surface waves transmission in material layers with imperfect interface", *Mater. Res. Express*, **6**(10), 105713. https://doi.org/10.1088/2053-1591/ab40e2.

Sun, W. H., Ju, G.L., Pan, J.W. and Li, Y.D. (2011), "Effects of the imperfect interface and piezoelectric/piezomagnetic stiffening on the SH wave in a multiferroic composite", *Ultrasonics*, **51**(7), 831-838. https://doi.org/10.1016/j.ultras.2011.04.002.

Tian, R., Liu, J., Pan, E. and Wang, Y. (2020), "SH waves in multilayered piezoelectric semiconductor plates with imperfect interfaces", *Eur. J. Mech. A - Solid*, **81**, 103961. https://doi.org/10.1016/j.euromechsol.2020.103961.

Ting, T. (2004), "Surface waves in a rotating anisotropic elastic half-space", *Wave Motion*, **40**(4), 329-346. https://doi.org/10.1016/j.wavemoti.2003.10.005.

Van Suchtelen, J. (1972), "Product properties: a new application of composite materials", *Phillips Res. Reports*, **27**, 28-37.

Van Run, A.M., Terrell, D.R. and Scholing, J.H. (1974), "An in situ grown eutectic magnetoelectric composite material: Part 2 physical properties", *J. Mater. Sci.*, **9**, 1710-1714. https://doi.org/10.1007/BF00540771.

Vinyas, M. (2021), "Computational analysis of smart magneto-electro-elastic materials and structures: review and classification", *Arch. Comput. Method. Eng.*, **28**(3), 1205-1248. https://doi.org/10.1007/s11831-020-09406-4.

Wu, C.P., Chen, S.J. and Chiu, K.H. (2010), "Three-dimensional static behavior of functionally graded magneto-electro-elastic plates using the modified Pagano method", *Mech. Res. Commun.*, **37**(1), 54-60. https://doi.org/10.1016/j.mechrescom.2009.10.003.

Yang, Z.X., Dang, P.F., Han, Q.K. and Jin, Z.H. (2018), "Natural characteristics analysis of magneto-electro-elastic multilayered plate using analytical and finite element method", *Compos. Struct.*, **185**, 411-420. https://doi.org/10.1016/j.compstruct.2017.11.031.

Zhao, L. and Chen, W.Q. (2010), "Plane analysis for functionally graded magneto-electro-elastic materials via the symplectic framework", *Compos. Struct.*, **92**(7), 1753-1761. https://doi.org/10.1016/j.compstruct.2009.11.029.

## Appendix

$$s=\frac{\alpha+\sqrt{\alpha^2-4\overline{C_{44}^{(m0)}}\left[\rho^{(m0)}\left(k^2c^2+\Omega^2+2i\Omega kc\right)-k^2\overline{C_{44}^{(m0)}}-k^2P^{(m0)}\right]}}{2\overline{C_{44}^{(m0)}}},$$

$$t=\frac{\alpha+\sqrt{\alpha^2-4k^2}}{2},$$

$$\gamma_{11}=\left(\overline{C_{44}^{(m0)}}+\zeta e_{15}^{(m0)}+\eta h_{15}^{(m0)}\right)\left(-s-g'ik\right)e^{-sg},$$

$$\gamma_{12}=e_{15}^{(m0)}\left(-t-g'ik\right)e^{-tg},\gamma_{55}=-e^{kg},$$

$$\gamma_{13}=h_{15}^{(m0)}\left(-t-g'ik\right)e^{-tg},\gamma_{34}=-e^{kg},$$

$$\gamma_{21}=\left(\zeta\kappa_{11}^{(m0)}-\eta\beta_{11}^{(m0)}\right)se^{(\alpha-s)g},$$

$$\gamma_{22}=t\kappa_{11}^{(m0)}e^{(\alpha-t)g},\gamma_{23}=t\beta_{11}^{(m0)}e^{(\alpha-t)g},$$

$$\gamma_{24}=k\kappa_{v}e^{kg},\gamma_{31}=\zeta e^{-sg},\gamma_{32}=e^{-tg},$$

$$\gamma_{41}=\left(\zeta\beta_{11}^{(m0)}+\eta\mu_{11}^{(m0)}\right)se^{(\alpha-s)g},$$

$$\gamma_{42}=t\beta_{11}^{(m0)}e^{(\alpha-t)g},\gamma_{43}=t\mu_{11}^{(m0)}e^{(\alpha-t)g},$$

$$\gamma_{45}=k\mu_{v}e^{kg},\gamma_{51}=\eta e^{-sg},\gamma_{53}=e^{-tg},$$

$$\gamma_{14}=\gamma_{15}=\gamma_{25}=\gamma_{33}=\gamma_{35}=\gamma_{44}=\gamma_{52}=\gamma_{54}=0.$$

$$\delta_{11}=\gamma_{11},\delta_{12}=\gamma_{12},\delta_{13}=\gamma_{13},\delta_{21}=\gamma_{31},\delta_{22}=\gamma_{32},$$
$$\delta_{23}=\gamma_{33},\delta_{31}=\gamma_{51},\delta_{32}=\gamma_{52},\delta_{33}=\gamma_{53}.$$

## Nomenclature

| | |
|---|---|
| $\rho$ | mass density |
| $T_{ij}$ | stress tensor |
| $u_i$ | Displacement vector components |
| $D_i$ | $i^{\text{th}}$-directed electric displacements |
| $B_i$ | $i^{\text{th}}$-directed magnetical displacements |
| $C_{ij}$ | elastic constant |
| $e_{ij}$ | piezoelectric constant |
| $\kappa_{ij}$ | dielectric constants |
| $\mu_{ij}$ | magnetic permittivity |
| $h_{ij}$ | piezomagnetic constants |
| $\beta_{ij}$ | electromagnetic constants |
| $S_{ij}$ | strain tensor |
| $E_i$ | elastic field intensity |
| $H_i$ | magnetic field intensity |
| $\phi_i$ | electrostatic potential |
| $\psi_i$ | magnetic potential |
| $k\left(=\frac{2\pi}{\lambda}\right)$ | wave number |
| $\lambda$ | wavelength |
| $c$ | phase velocity |
| $\Omega$ | rotation parameter |
| $a$ | corrugation amplitude |
| $\boldsymbol{\Omega}\times\boldsymbol{\Omega}\times\boldsymbol{u}$ | Centripetal acceleration |
| $2\boldsymbol{\Omega}\times\dot{\boldsymbol{u}}$ | Coriolis acceleration |
| $\alpha$ | functional gradient parameter |